Fluid-Structure Interaction.
Theory, Numerics and Applications
pp. 21– 30
Herrsching am Ammersee, 29.9.-1.10.2008

On Coupling Schemes for Heat Transfer in FSI Applications

P. Birken, K. J. Quint, S. Hartmann, A. Meister

In this article, the coupling of the temperature-dependent, compressible Navier-Stokes equations solved by a compressible finite volume scheme together with the finite element solution of the heat equation is considered. The application is focused on the cooling process of a heated metal bar treated in the field of metal forming technology. This is done both by loose and strong numerical coupling methods based on the Backward-Euler scheme, where, particularly, Gauss-Seidel and fixed-point solvers are considered.

Keywords: Fluid-Structure Interaction, Thermal Coupling, Partitioned Approach

1 Introduction

Many industrial applications of metal forming involve a simultaneous or subsequent heat treatment. The purpose of this treatment is to improve the mechanical properties such as ductility, hardness, yield strength, or impact resistance. For this purpose the steel is heated up to a certain temperature (austenitic temperature) and then cooled with a critical rate. The thermal evolution (cooling rate) defines the final material properties and, accordingly, its prediction is of particular interest. This complicated process has to be handled by numerical simulations implying thermo-mechanical coupling effects in the gas (fluid-mechanical part), which is used for cooling the metal specimen, the heat transport within the solid (solid mechanical part) and thermo-mechanical coupling effects in the solid itself. The mechanical effects are out of the scope of the investigations here. We will treat the heat transfer from the solid region into the fluid region through a fluid-structure interaction problem.

In our application a metal bar is heated and then cooled at the surface by cold compressed air. This results in an unsteady thermal coupling problem, where the hot steel heats the cold air, which is of low to medium speed. The effect of radiation is neglected for the purpose of getting a more clear picture of the numerical methods with a special focus on the coupling procedure.

Thus, we will look at a model problem, which serves as a stepping stone for further work: the compressible Navier-Stokes-equations as a model for air, coupled along a non-moving boundary with the heat equation as a model for the temperature distribution in the steel. While a lot of work has been done on the thermal coupling of incompressible fluids with structure, we are looking at thermal coupling of a compressible fluid and a structure. Research on numerical simulation of this problem was so far mainly driven by problems where hot gas heats the structure, for example supersonic reentry of vehicles from space or heating of gas-turbine blades (Hinderks and Radespiel, 2006; Mehta, 2005). The results are mainly qualitative, describing numerical methods and the comparison of numerical results to experimental data, with the conclusion that the results are not always in agreement with experiments (Hinderks and Radespiel, 2006).

For the fluid-structure interaction, we consider a partitioned approach (Farhat, 2004), where different codes are used for the subproblems and the coupling is done by a master program which calls by interface functions the other codes. This allows to use existing software for the subproblems, by contrast to a monolithic approach, where a new code is tailored for the coupled equations. This problem is solved numerically using a finite volume method (FVM) for the fluid and a finite element method (FEM) for the heat equation as the methods for space-discretization. Another distinction is made between loose coupling and strong coupling approaches. In the first approach, only one step of each solver is performed in each time step, while the latter approach adds a convergence criterion and an inner loop. We will consider both loose and strong coupling and compare the results on the thermal coupling problem.

The method of lines then implies the time-discretization, where it is common to apply low order time integration in both methods, FVM and FEM, respectively and in the coupling solver.

2 Governing equations and discretization

In the following a thermal coupling problem is considered, where a fluid domain $\Omega_1 \subset \mathbb{R}^2$ and a structure domain $\Omega_2 \subset \mathbb{R}^2$ are given. Within the Ω_1-domain use is made of the temperature-dependent Navier-Stokes equations for compressible flow consisting of the continuity equation, the balance of momentum and the energy relation to describe the thermally coupled fluid flow. In the Ω_2-domain the transient heat equation is assumed. The domains meet at an interface Γ consisting of a curve in $\mathbb{R}^2$, where we require that temperature and heat flux are continuous. No further coupling conditions of the interface are taken into account. For the fluid use is made of the DLR TAU-Code, see (Gerhold et al., 1997), and for the structural part the in-house FEM-program TASAFEM for high-order time-integration is applied, see both (Hartmann, 2006) and, for example, (Hartmann, 2002).

To comply with the condition that temperature and heat flux are continuous at the interface Γ, a so-called Dirichlet-Neumann-coupling is used. Namely, the boundary conditions for the two solvers are chosen such that we prescribe Neumann data for one solver and Dirichlet data for the other. Following the analysis of Giles (1997), temperature is prescribed for the equation with smaller heat conductivity, namely the fluid and heat flux for the structure. Convergence of this approach has been proved for a system of coupled Laplace equations, but not for the case considered here.

2.1 Structure Discretization

The finite element code TASAFEM is a high-order time-integration program originally based on stiffly accurate, diagonally implicit Runge-Kutta methods, see (Ellsiepen and Hartmann, 2001), here extended to the unsteady heat conduction case. The heat conduction problem is, although unsteady, in a first approximation linear. We start from the balance of energy

$$\rho(\boldsymbol{x}) c_D \dot{\Theta}(\boldsymbol{x}, t) = -\operatorname{div} \boldsymbol{q}(\boldsymbol{x}, t), \tag{1}$$

where $\boldsymbol{x}$ defines the spatial coordinates and t the time. The dot symbolizes the time derivative and

$$\boldsymbol{q}(\boldsymbol{x}, t) = -\lambda \operatorname{grad} \Theta(\boldsymbol{x}, t)$$

denotes the heat flux vector depending by Fourier's law on the coefficient of heat conduction λ (which is assumed to define an isotropic heat conductivity). Furthermore, $\Theta(\boldsymbol{x}, t)$ is the absolute temperature, $\rho(\boldsymbol{x})$ the density and c_D denotes the specific heat at constant deformation. On the boundary, we have Neumann conditions, where the heat flux $\boldsymbol{q}(\boldsymbol{x}, t) \cdot \boldsymbol{n}(\boldsymbol{x}) = q(\boldsymbol{x}, t)$ is given on ∂A^q with the outer normal vector $\boldsymbol{n}(\boldsymbol{x})$. Furthermore, initial conditions $\Theta(\boldsymbol{x}, 0) = \Theta_0(\boldsymbol{x})$ are required.

In view of the classical finite element setting, multiplying Eq. (1) with a virtual temperature field $\delta\Theta(\boldsymbol{x})$, the weak formulation reads

$$\int_{\Omega_2} \rho c_D \dot{\Theta} \delta\Theta \, \mathrm{d}V = -\int_{\Omega_2} \lambda \operatorname{grad} \Theta \operatorname{grad} \delta\Theta \, \mathrm{d}V - \int_{\partial A^q} q \delta\Theta \, \mathrm{d}A. \tag{2}$$

Next, one inserts an ansatz

$$\Theta^h(\boldsymbol{x}, t) = \boldsymbol{N}^T(\boldsymbol{x}) \, \boldsymbol{\Theta}(t) \tag{3}$$

$$\delta\Theta^h(\boldsymbol{x}) = \boldsymbol{N}^T(\boldsymbol{x}) \, \delta\boldsymbol{\Theta} \tag{4}$$

into Eq. (2). The temperature gradient reads in matrix notation

$$\operatorname{grad} \Theta^h = \left\{ \begin{array}{c} \partial_{x_1} \Theta^h \\ \partial_{x_2} \Theta^h \end{array} \right\} = \left\{ \begin{array}{c} \boldsymbol{N}_{,1}^T \\ \boldsymbol{N}_{,2}^T \end{array} \right\} \boldsymbol{\Theta}(t) = \boldsymbol{B}(\boldsymbol{x}) \boldsymbol{\Theta}(t) \tag{5}$$

with the temperature gradient- nodal temperature matrix $\boldsymbol{B}(\boldsymbol{x})$. If we insert ansatz (3) and (4) into the weak formulation (2), we obtain a system of ordinary differential equations

$$\boldsymbol{g}(t, \boldsymbol{\Theta}, \dot{\boldsymbol{\Theta}}) = \boldsymbol{M} \dot{\boldsymbol{\Theta}}(t) + \boldsymbol{K}(\boldsymbol{\Theta}) \boldsymbol{\Theta}(t) - \bar{\boldsymbol{q}}(t, \underline{\boldsymbol{u}}) = \boldsymbol{0}. \tag{6}$$

The heat flux on the coupling boundary is defined by

$$\bar{\boldsymbol{q}}(t,\underline{\boldsymbol{u}}) = -\int_{\partial A^q} \boldsymbol{N}\, \boldsymbol{q}^h(t,\underline{\boldsymbol{u}})\, \mathrm{d}A, \tag{7}$$

where $\underline{\boldsymbol{u}}$ was introduced to denote the dependence on the fluid data as explained in the next section.

$$\boldsymbol{M} = \int_{\Omega_2} \rho c_D \boldsymbol{N}\,\boldsymbol{N}^T\, \mathrm{d}V \qquad \boldsymbol{K} = \int_{\Omega_2} \lambda(\Theta^h)\boldsymbol{B}^T\boldsymbol{B}\, \mathrm{d}V \tag{8}$$

are the matrices concerned. In the case of a constant domain, no volumetric distributed heat sources and temperature-independent material parameters, a Backward-Euler step of Eq.(6) reads

$$[\boldsymbol{M} + \Delta t_n\, \boldsymbol{K}]\, \boldsymbol{\Theta}^{n+1} = \boldsymbol{M}\boldsymbol{\Theta}^n + \bar{\boldsymbol{q}}(t_{n+1}, \underline{\boldsymbol{u}}^{n+1}) \tag{9}$$

implying the solution of a symmetric, sparse linear system of equations to obtain the nodal temperatures at time t_{n+1}.

2.2 Fluid discretization

Concerning the fluid part, the flow is assumed to be governed by the two dimensional temperature-dependent compressible Navier-Stokes equations. The common non-dimensional integral form of the corresponding conservation laws reads

$$\frac{d}{dt}\int_\sigma \boldsymbol{u}\mathrm{d}V + \sum_{j=1}^{2}\int_{\partial\sigma} \boldsymbol{f}_j^c(\boldsymbol{u})\, n_j \mathrm{d}A = \frac{1}{\mathrm{Re}_\infty}\sum_{j=1}^{2}\int_{\partial\sigma} \boldsymbol{f}_j^v(\boldsymbol{u})\, n_j \mathrm{d}A, \tag{10}$$

where $\boldsymbol{n} = \{n_1, n_2\}^T$ represents the outwards unit normal vector at the boundary of the control volume σ. Furthermore,

$$\boldsymbol{u} = \{\rho, \rho v_1, \rho v_2, \rho E\}^T$$

is the vector of the conserved variables and $\boldsymbol{f}_j^c, \boldsymbol{f}_j^v, j = 1, 2$ are the convective and viscous fluxes which are given by

$$\boldsymbol{f}_j^c(\boldsymbol{u}) = \begin{Bmatrix} \rho v_j \\ \rho v_1 v_j + \delta_{1j} p \\ \rho v_2 v_j + \delta_{2j} p \\ \rho H v_j \end{Bmatrix} \text{ and } \boldsymbol{f}_j^v(\boldsymbol{u}) = \begin{Bmatrix} 0 \\ \tau_{1j} \\ \tau_{2j} \\ \sum_{i=1}^2 v_i\tau_{ij} + \frac{\mu\gamma}{\mathrm{Pr}_\infty}\partial_{x_j} e \end{Bmatrix},$$

respectively. The quantity e denotes the internal energy, which is given by $e = E - 1/2\left(v_1^2 + v_2^2\right)$ and H is defined by $H = E + p/\rho$. The pressure is determined by the equation of state $p = (\gamma-1)\rho\left(E - 1/2\left(v_1^2 + v_2^2\right)\right)$, where γ denotes the ratio of specific heats. The temperature is given by $\Theta = \gamma(\gamma-1)\mathrm{Ma}_\infty^2 e$, where Ma_∞ denotes the Mach number at infinity. The elements of the shear stress tensor are

$$\tau_{ij} = \mu\left(\partial_{x_j} v_i + \partial_{x_i} v_j\right) + \delta_{ij}\tilde{\lambda}\left(\partial_{x_1} v_1 + \partial_{x_2} v_2\right),$$

with the viscosity assumed to follow the Sutherland law $\mu = \Theta^{1.5}(1+S)/(\Theta+S)$, where $S = 110K/\Theta_\infty$ and Θ_∞ denote the temperature at infinity measured in degree of Kelvin. Moreover, the relation between the thermal conductivity and the viscosity is defined by the Stokes' hypothesis to be $\tilde{\lambda} = -2/3\mu$ and Re_∞ and Pr_∞ denote the Reynolds and Prandtl number at infinity, respectively.

In order to solve (10) numerically, we consider a conforming triangulation $\mathcal{T}_h$ of the spatial domain is the sense of Delaunay, see (Friedrich, 1993). Based on this primary grid, we define a discrete control volume σ_i as the volume of the barycentric subdivision of $\mathcal{T}_h$ enclosing the node $\boldsymbol{x}_i = \{x_{i1}, x_{i2}\}^T$ and bounded by the straight line segments l_{ij}^k connecting the midpoint of the edge with the inner point $\boldsymbol{x}_s$ (see Fig. 1). For a detailed description, we refer to Meister and Sonar (1998). Utilizing our notion of control volumes and introducing the cell average on σ_i by $\boldsymbol{u}_i(t) := \int_{\sigma_i} \boldsymbol{u}(\boldsymbol{x},t)\mathrm{d}V/|\sigma_i|$ into the Navier-Stokes equations (10), we obtain the form

$$\dot{\boldsymbol{u}}_i(t) = \frac{1}{|\sigma_i|}\sum_{j\in N(i)}\sum_{k=1}^{2}\int_{l_{ij}^k}\sum_{\ell=1}^{2}\left(\frac{1}{\mathrm{Re}_\infty}\boldsymbol{f}_\ell^v(\boldsymbol{u}) - \boldsymbol{f}_\ell^c(\boldsymbol{u})\right) n_\ell \mathrm{d}A,$$

where $N(i)$ denote the index set of all control volumes σ_j neighboring box σ_i. To overcome the difficulty that the line integrals are usually not defined if $\boldsymbol{u}$ is discontinuous, we introduce the concept of numerical flux functions.

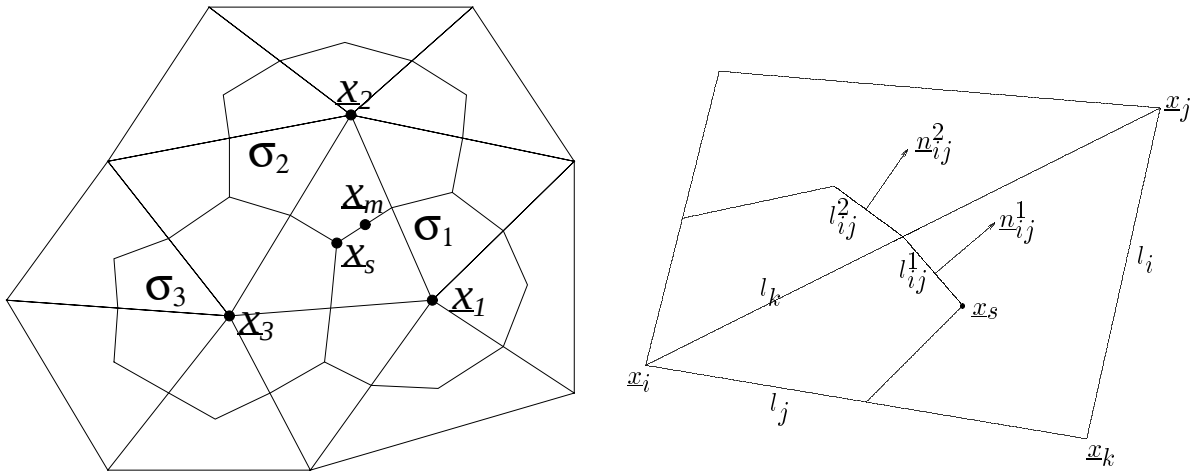

(a) Triangulation $\mathcal{T}_h$ (b) Boundary lines

Figure 1: General form of a control volume

Concerning the convective part, we make use of the well-known AUSMDV scheme, see (Wada and Liou, 1994). Furthermore, the viscous fluxes are discretized by central differences. Therefore, for each physical quantity ϕ appearing within the viscous flux, the unique linear distribution with respect to the triangle τ is calculated by means of the cell averages of the three adjacent control volumes σ_i satisfying $\sigma_i \cap \tau \neq \emptyset$. In this procedure the cell averages are considered to be located at the vertices of the triangle. Due to this reconstruction the value as well as the gradient of each quantity can easily be evaluated at the midpoint of the inner line segment $l_{ij}^k \subset \tau$. Thus, the semi-discrete form of the governing equations reads

$$\dot{\boldsymbol{u}}_i(t) = \frac{1}{|\sigma_i|} \sum_{j \in N(i)} \sum_{k=1}^{2} |l_{ij}^k| \left(\boldsymbol{h}^v(\boldsymbol{u}_i^{n+1}, \boldsymbol{u}_j^{n+1}, \boldsymbol{u}_m^{n+1}; \boldsymbol{n}_{ij}^k) - \boldsymbol{h}^c(\hat{\boldsymbol{u}}_i^{n+1}, \hat{\boldsymbol{u}}_j^{n+1}; \boldsymbol{n}_{ij}^k) \right),$$

where $\boldsymbol{h}^c$ is the AUDMDV flux and $\boldsymbol{h}^v$ corresponds to the discretization of the viscous fluxes. Note that the notation $\hat{\boldsymbol{u}}_i$ emphasizes that we increase the order of accuracy for the convective part by utilizing a well-known TVD-like reconstruction technique and, accordingly, $\hat{\boldsymbol{u}}_i$ denotes the one-sided limit with respect to the box σ_i at the midpoint of the line segment l_{ij}^k. If we write this as an equation for the complete domain, we obtain

$$\dot{\underline{\boldsymbol{u}}}(t) = \boldsymbol{\sigma}^{-1} \underline{\boldsymbol{h}}(\underline{\boldsymbol{u}}, \boldsymbol{\Theta}). \tag{11}$$

The underlined vectors represent the respective vectors on the whole fluid grid and we have included the dependence on the structural temperature on the coupling interface through the vector of the structure temperatures $\boldsymbol{\Theta}$. The matrix $\boldsymbol{\sigma}$ is a diagonal matrix with the volumes of the corresponding cells on the diagonal.

Similar to TASAFEM the restrictive time-step constraint of an explicit discretization technique for the time derivative is overcome using an Backward-Euler approach. Thus, the discrete form of the governing equations reads

$$\underline{\boldsymbol{u}}^{n+1} = \underline{\boldsymbol{u}}^n + \Delta t_n \boldsymbol{\sigma}^{-1} \underline{\boldsymbol{h}}(\underline{\boldsymbol{u}}^{n+1}, \boldsymbol{\Theta}^{n+1}), \tag{12}$$

where $\underline{\boldsymbol{u}}^{n+1} \approx \underline{\boldsymbol{u}}(t_{n+1})$ and $t_{n+1} = t_n + \Delta t_n$. It is easily seen that each time step within the fluid solver requires the solution of a sparse non-linear system of equations, which is performed by a dual time-stepping approach, see (Jameson, 2004). The precise choice of the solver for this non-linear system is not important here, so instead, a Newton-Krylov method could be used.

2.3 Coupled equations

If we combine the semidiscrete equations (6) for the domain Ω_1 and (11) for the domain Ω_2, we obtain a coupled system of ODEs

$$\begin{aligned} \dot{\underline{\boldsymbol{u}}}(t) &= \boldsymbol{\sigma}^{-1} \underline{\boldsymbol{h}}(\underline{\boldsymbol{u}}, \boldsymbol{\Theta}), \\ \boldsymbol{M} \dot{\boldsymbol{\Theta}}(t) &= -\boldsymbol{K} \boldsymbol{\Theta}(t) - \bar{\boldsymbol{q}}(t, \underline{\boldsymbol{u}}), \end{aligned} \tag{13}$$

where we prescribe the additional algebraic constraint that temperature and heat flux are continuous at the coupling interface Γ. The application of the Backward-Euler method to the coupled system is straightforward. The question is now, how the coupled system can be solved accurately and efficiently.

3 Fluid-Structure-Coupling

As described above, we pursue a partitioned approach. The technical difficulty of different programming languages (FORTRAN for TASAFEM and C++ for TAU) in the partitioned approach is dealt by means of the C++-library called Component Template Library (CTL), see (Matthies et al., 2006).

It is assumed that at time t_n the fluid data $\underline{\boldsymbol{u}}^n$, the structure data $\boldsymbol{\Theta}^n$ and a global step-size Δt_n are given. As described above, the fluid and the structural equations are both treated implicitly with associated solvers for the time-stepping procedure. In the coupling context, it is useful to regard the two solvers as mappings that, for given fixed data $\underline{\boldsymbol{u}}^n$ at t_n, respectively $\boldsymbol{\Theta}^n$, take an approximation of the boundary data at t_{n+1} from the other solver and provide a new approximation to their data at t_{n+1}, which provides new boundary data for the other solver. The fluid solver provides a solution to (12) and can be written as

$$\underline{\boldsymbol{u}}^{n+1} = \boldsymbol{F}(\boldsymbol{P}(\boldsymbol{\Theta})),$$

whereas the structure solver provides a solution to (9) and can be represented by

$$\boldsymbol{\Theta}^{n+1} = \boldsymbol{S}(\boldsymbol{q}_\Gamma(\underline{\boldsymbol{u}})).$$

$\boldsymbol{P}$ is a projection of the temperature onto the boundary of Ω_2 and $\boldsymbol{q}_\Gamma$ provides the boundary heat flux in the fluid. Using this notation, it is possible to define coupling methods. The most simple coupling procedures are loose coupling methods, where no convergence criterion is used in the coupling iteration. In particular, there is Gauss-Seidel coupling

$$\underline{\boldsymbol{u}}^{n+1} = \boldsymbol{F}(\boldsymbol{P}(\boldsymbol{\Theta}^n)), \tag{14}$$
$$\boldsymbol{\Theta}^{n+1} = \boldsymbol{S}(\boldsymbol{q}_\Gamma(\underline{\boldsymbol{u}}^{n+1})), \tag{15}$$

and Jacobi-coupling, which can be done in parallel:

$$\underline{\boldsymbol{u}}^{n+1} = \boldsymbol{F}(\boldsymbol{P}(\boldsymbol{\Theta}^n)), \tag{16}$$
$$\boldsymbol{\Theta}^{n+1} = \boldsymbol{S}(\boldsymbol{q}_\Gamma(\underline{\boldsymbol{u}}^n)). \tag{17}$$

These can be iterated leading to fixed point coupling, here for the Gauss-Seidel case:

$$\underline{\boldsymbol{u}}_{k+1}^{n+1} = \boldsymbol{F}(\boldsymbol{P}(\boldsymbol{\Theta}_k^{n+1})), \tag{18}$$
$$\boldsymbol{\Theta}_{k+1}^{n+1} = \boldsymbol{S}(\boldsymbol{q}_\Gamma(\underline{\boldsymbol{u}}_{k+1}^{n+1})), \quad k = 0, 1, \ldots. \tag{19}$$

As a fixed point equation this is given by

$$\boldsymbol{P}(\boldsymbol{\Theta}) = \boldsymbol{P}(\boldsymbol{S}(\boldsymbol{q}_\Gamma(\boldsymbol{F}(\boldsymbol{P}(\boldsymbol{\Theta}))))), \tag{20}$$

which can be used as a convergence criterion for the fixed point iteration. Various methods have been proposed to increase the convergence speed of the fixed point iteration by decreasing the interface error between subsequent steps, for example Relaxation (Le Tallec and Mouro, 2001; Küttler and Wall, 2008), Interface-GMRES (Michler et al., 2006) or ROM-coupling (Vierendeels et al., 2007). For the purpose of looking at the qualitative behavior of loose and strong coupling, it is sufficient to analyze the more simple methods described here.

4 Numerical Results

4.1 Test case

To analyze the properties of the coupling method, the test example is chosen as simple as possible. The reason is that this comparably simple coupling problem is already beyond the current solution theory, respectively convergence theory of numerical methods. Therefore, we choose a test case where the exact solutions for the uncoupled problems are known in order to make sure that no additional side effects are present, which cannot be controlled.

Accordingly, the cooling of a flat plate resembling a simple work piece is considered (described in Fig. 2 as solid). This example has also been studied by other authors (Yarrington and Thornton, 1994) and (Huebner et al., 2001, p. 465) in conjunction with the cooling of structural parts in hypersonic vehicles. There localized heating was of special interest. In our case the work piece is initially at a temperature of $\Theta(\boldsymbol{x}, 0) = 900$ K and is cooled by a constant air stream. The latter is modeled in a first approximation as a laminar flow along the plate, see Fig. 2. For

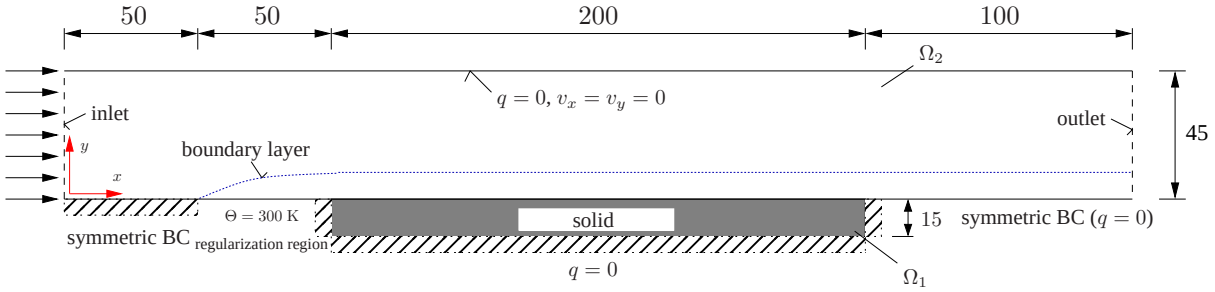

Figure 2: Test case for the coupling method

the work piece the following constant material properties are assumed: mass density $\rho = 7836\ \mathrm{kg/m^3}$, specific heat capacity $c_D = 443\ \mathrm{J/(kgK)}$ and thermal conductivity $\lambda = 48.9\ \mathrm{W/(mK)}$. The inlet is at the left, where the air enters the domain with an initial velocity of $\mathrm{Ma}_\infty = 0.8$ in horizontal direction and a temperature of 273 K. Then, there are two succeeding regularization regions of $50\ \mathrm{mm}$ to obtain an unperturbed boundary layer. In the first region, $0 \leq x \leq 50$, symmetry boundary conditions, $v_y = 0$, $q = 0$, are applied. In the second region, $50 \leq x \leq 100$, a constant wall temperature of 300 K is specified. Within this region the velocity boundary layer fully develops. The third part is the solid (work piece) of length $200\ \mathrm{mm}$, which exchanges heat with the fluid, but is assumed insulated otherwise, $q = 0$. Therefore, the corresponding Neumann boundary conditions are applied throughout. Finally, the flow domain is closed by a second regularization region of $100\ \mathrm{mm}$ with symmetry boundary conditions and the outlet.

The grid, see Fig. 3, in the structural part is chosen cartesian and equidistant, whereas the thinnest cells in the fluid

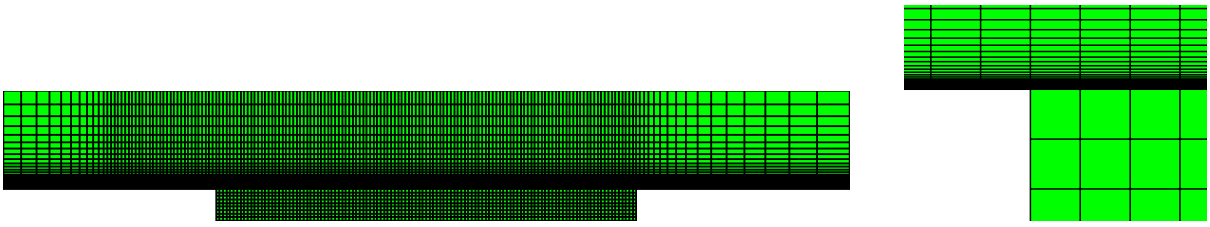

(a) Entire mesh (b) Mesh zoom

Figure 3: Full grid (left) and zoom into coupling region (right)

region have an aspect ratio of 1:200 and then become coarser in y-direction. The points of the primary fluid grid and the nodes of the structure grid match on the interface, which avoids additional difficulties from interpolation. Thus, we have 9660 cells in the fluid region and $n_x \times n_y = 120 \times 9 = 1080$ elements with $121 \times 10 = 1210$ nodes in the region of the structure.

To specify reasonable initial conditions within the fluid a steady state solution of the flow with constant wall temperature is computed. To cope with convergence problems we first compute a solution with a medium boundary temperature. In a second step the temperature at the boundary is increased up to the value $\Theta = 900$ K. Due to the constant boundary temperature we are able to compare the results with the theoretical solution of Blasius for the velocity boundary layer and of van Driest for the temperature boundary layer (Van Driest, 1952) and thereby verify the quality of our grid and our fluid solver. In the structure, a constant temperature of 900 K at $t = 0$ s is chosen throughout.

4.2 Numerical tests

In Fig. 4 one can see the temporal evolution of the temperature at the middle of the coupling interface. As expected,

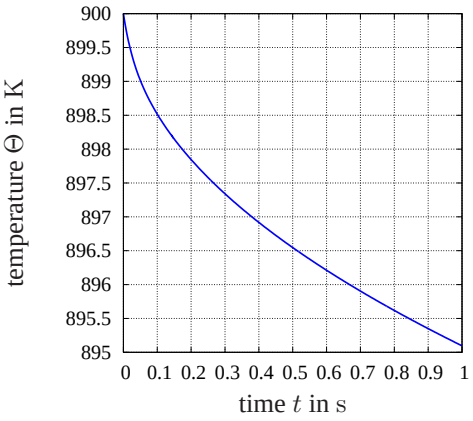

Figure 4: Temperature evolution at the middle point of the interface

the temperature decreases monotonously with a large gradient at the beginning of the process, which decreases in the following. At $t = 1$ s, the temperature has dropped down from 900 K to approximately 895 K. This solution is obtained using fixed point coupling and $\Delta t_n = 0.0025$ s. Since no exact solution is available, it will be used as reference solution.

As for strong coupling methods, the fixed point method is iterated until the vector 2-norm of the interface residual (20) has dropped below $\epsilon = 0.1$, i.e. $\left\| \boldsymbol{P}\left(\boldsymbol{\Theta}_{k+1}^{n+1}\right) - \boldsymbol{P}\left(\boldsymbol{\Theta}_{k}^{n+1}\right) \right\|_2 \leq \epsilon$. As mentioned before $\boldsymbol{P}$ is a projection of the temperature onto the boundary and k is the iteration number of the fixed point iteration. Except for the first time-step, two iterations are sufficient to fulfill this criterion. In this case, for $\Delta t = 0.1$ s and $\Delta t = 0.05$ s, three iterations are needed.

Next, the Gauss-Seidel coupling is compared with the iterated Gauss-Seidel (fixed point) coupling for time step sizes Δt of 0.1 s, 0.05 s and 0.025 s. To this end, we consider the resulting error at $t = 1$ s, using the 2-norm of the difference of temperatures at the interface to the reference solution. In Fig. 5(a) one can see the error over the

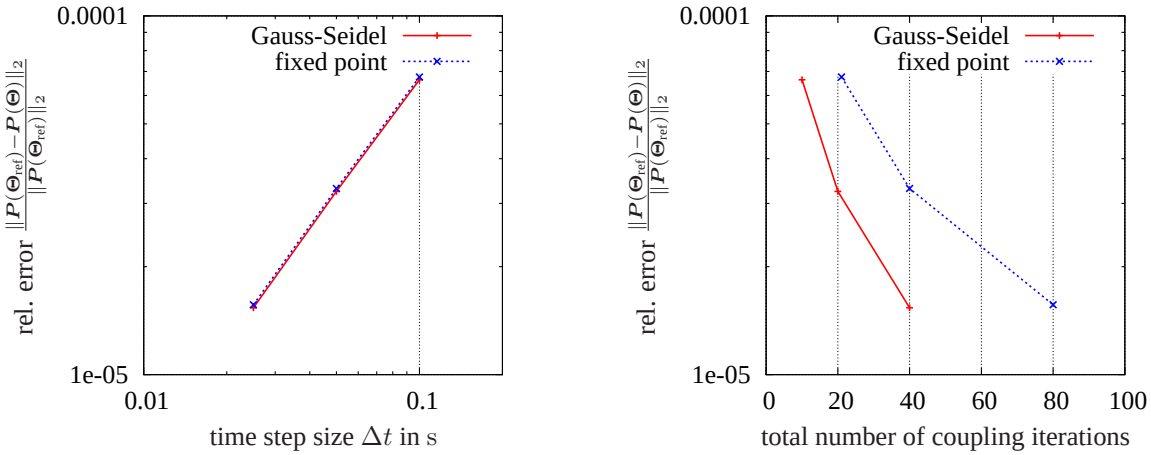

(a) Relative error over time-steps

(b) Relative error over coupling iterations

Figure 5: Relative error behavior

time step size and in Fig. 5(b), compared to the number of coupling iterations. As can be seen, in the investigated application fixed point coupling does not improve the accuracy of the solution if $\epsilon = 0.1$ is employed as dropping tolerance. The relative error of the numerical method is practically unaltered but the computational cost is at least doubled, depending on the specified tolerance ϵ of the fixed point coupling. On the other hand the time step size Δt has, as expected, a significant influence on the accuracy.

5 Conclusions

The coupling of the temperature-dependent compressible Navier-Stokes equations using a finite volume code and the heat equation using finite elements, both based on a Backward-Euler time-integration step, are considered. In the investigated test example the fluid cools the structure. We compare loose to strong coupling methods for this problem occurring in the field of hot metal forming processes and it can be seen that for a simple example of a plain metal specimen and a dropping tolerance of $\epsilon = 0.1$, loose coupling methods are completely sufficient.

Acknowledgements

We would like to thank Dr. Volker Hannemann from the DLR Göttingen for his help with the TAU-Code and Dr. Rainer Niekamp from the TU Braunschweig supporting us with the usage of CTL. This paper is based on investigations of the collaborative research center SFB/TR TRR 30, which is kindly supported by the German Research Foundation (DFG)

References

Ellsiepen, P.; Hartmann, S.: Remarks on the interpretation of current non-linear finite-element-analyses as differential-algebraic equations. *Int. J. Num. Meth. Eng.*, 51, (2001), 679–707.

Farhat, C.: CFD-based nonlinear computational aeroelasticity. In: E. Stein; R. de Borst; T. J. Hughes, eds., *Encyclopedia of Computational Mechanics, Volume 3: Fluids*, pages 459–480, John Wiley and Sons (2004).

Friedrich, O.: A new method for generating inner points of triangulations in two dimensions. *Comp. Meth. Appl. Mech. Eng.*, 104, (1993), 77–86.

Gerhold, T.; Friedrich, O.; Evans, J.; Galle, M.: Calculation of complex three-dimensional configurations employing the DLR-TAU-Code. *AIAA Paper*, 97-0167.

Giles, M.: Stability analysis of numerical interface conditions in fluid-structure thermal analysis. *Int. J. Num. Meth. in Fluids*, 25, (1997), 421–436.

Hartmann, S.: Computation in finite strain viscoelasticity: finite elements based on the interpretation as differential-algebraic equations. *Comp. Meth. Appl. Mech. Eng.*, 191, 13-14, (2002), 1439–1470.

Hartmann, S.: TASA-FEM: Ein Finite-Elemente-Programm für raum- und zeitadaptive gekoppelte Strukturberechnungen. Tech. Rep. 1/2006, Institute of Mechanics, University of Kassel, Kassel, Germany (2006).

Hinderks, M.; Radespiel, R.: Investigation of hypersonic gap flow of a reentry nosecap with consideration of fluid structure interaction. *AIAA Paper*, 06-1111.

Huebner, K. H.; Dewhirst, D. L.; Smith, D. E.; Byrom, T. G.: *The Finite Element Methods for Engineers*. John Wiley & Sons, 4th edn. (2001).

Jameson, A.: Aerodynamics. In: E. Stein; R. de Borst; T. J. Hughes, eds., *Encyclopedia of Computational Mechanics, Volume 3: Fluids*, pages 325–406, John Wiley and Sons (2004).

Küttler, U.; Wall, W.: Fixed-point fluid-structure interaction solvers with dynamic relaxation. *Comp. Mech.*, 43, (2008), 61–72.

Le Tallec, P.; Mouro, J.: Fluid structure interaction with large structural displacements. *Comp. Meth. Appl. Mech. Eng.*, 190, (2001), 3039–3067.

Matthies, H. G.; Niekamp, R.; Steindorf, J.: Algorithms for strong coupling procedures. *Comp. Meth. Appl. Mech. Eng.*, 195, (2006), 2028–2049.

Mehta, R. C.: Numerical computation of heat transfer on reentry capsules at mach 5. *AIAA-Paper 2005-178*.

Meister, A.; Sonar, T.: Finite-volume schemes for compressible fluid flow. *Surv. Math. Ind.*, 8, (1998), 1–36.

Michler, C.; van Brummelen, E.; de Borst, R.: Error-amplification analysis of subiteration-preconditioned GMRES for fluid-structure interaction. *Comp. Meth. Appl. Mech. Eng.*, 195, (2006), 2124–2148.

Van Driest, E.: National advisory commitee for aeronautics (naca) - investigation of laminar boundary layer in compressible fluids using the crocco method. *NACA*.

Vierendeels, J.; Lanoye, L.; Degroote, J.; Verdonck, P.: Implicit coupling of partitioned fluid-structure interaction problems with reduced order models. *Comp. & Struct.*, 85, (2007), 970–976.

Wada, Y.; Liou, M.-S.: A Flux Splitting Scheme with High-Resolution and Robustness for Discontinuities. *AIAA Paper*, 94–0083.

Yarrington, P. W.; Thornton, E. A.: Finite element analysis of low-speed compressible flows within convectively cooled structures. *Journal of Thermophysics and Heat Transfer*, 8–4.

Address: Dr. P. Birken (corresponding author), Department of Mathematics, University of Kassel, Heinrich-Plett Str. 40, 34132 Kassel, Germany. email: birken@mathematik.uni-kassel.de

Dipl.-Ing. K.-J. Quint, Institute of Mechanics, University of Kassel, Mönchebergstr. 7, 34105 Kassel, Germany. karsten.quint@uni-kassel.de

Prof. Dr.-Ing. St. Hartmann, Institute of Applied Mechanics, Clausthal University of Technology, Adolph-Roemer Str. 2a, 38678 Clausthal-Zellerfeld, Germany, email: stefan.hartmann@tu-clausthal.de

Prof. Dr. A. Meister, Department of Mathematics, University of Kassel, Heinrich-Plett Str. 40, 34132 Kassel, Germany. email: meister@mathematik.uni-kassel.de